JOURNAL OF MODERN OPTICS, 15 APRIL–10 MAY 2004
VOL. 51, NO. 6–7, 785–797

Taylor & Francis
Taylor & Francis Group

Decoherence effects in superradiant light scattering from a moving Bose-Einstein condensate

R. BONIFACIO†, F. S. CATALIOTTI‡, M. COLA†, L. FALLANI*, C. FORT*, N. PIOVELLA† and M. INGUSCIO*

INFM and European Laboratory for Non-Linear Spectroscopy (LENS) via N. Carrara 1, I-50019 Sesto F.no (FI), Italy
† also Dipartimento di Fisica, Università degli Studi di Milano, Via Celoria 16, I-20133 Milano, Italy
‡ also Dipartimento di Fisica, Università di Catania, via S. Sofia 64, I-95124 Catania, Italy
* also Dipartimento di Fisica, Università di Firenze, via G. Sansone 1, I-50019 Sesto F.no (FI), Italy

(*Received 18 November 2003; revision received 30 November 2003*)

Abstract. We present the results of an experiment on superradiant Rayleigh scattering from a moving Bose-Einstein condensate, where a superposition of two atomic wavepackets is created by the interaction of a far-detuned laser beam with the condensate. The system is described by the CARL-BEC model which is a generalization of the Gross-Pitaevskii model to include the self–consistent evolution of the scattered field. The experiment gives evidence of a damping of the matter-wave grating which depends on the initial velocity of the condensate. We describe this damping in terms of a phase-diffusion decoherence process, in good agreement with the experimental results. In a second experiment we add a seeding beam counterpropagating with respect to the pump beam. Varying intensity and frequency of the seed, we investigate the transition from the superradiant regime to the Rabi oscillations regime, evidencing fundamental differences between these two processes.

1. Introduction

The experimental realization of Bose-Einstein condensates (BECs) with alkali trapped atoms has opened the possibility of investigating several fundamental aspects of quantum mechanics in macroscopic, i.e. many particle systems [1]. In superradiant Rayleigh scattering the coherent nature of the condensate leads to strong correlations between successive scattering events, as shown in the early work by Ketterle and co-workers [2]. This process was the basis for the first demonstration of phase-coherent matter wave amplification [3]. The effect studied by Ketterle is an example of a spontaneous formation of a regular density grating in an atomic system, arising from a collective instability as in the Collective Atomic Recoil Laser (CARL) [4]. In the absence of thermal broadening (as is the case in a BEC), CARL appears as a promising source of macroscopically entangled or number-squeezed atom-atom and/or atom-photon systems [5–7]. However, in a real BEC effects such as spontaneous emission, inhomogeneous broadening and

Journal of Modern Optics ISSN 0950–0340 print/ISSN 1362–3044 online © 2004 Taylor & Francis Ltd
http://www.tandf.co.uk/journals
DOI: 10.1080/09500340410001664269

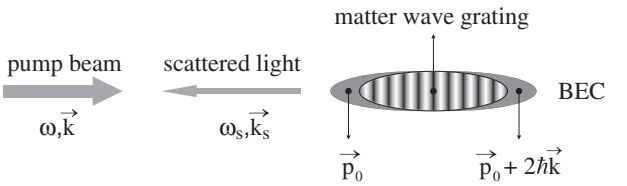

Figure 1. An elongated Bose-Einstein condensate is illuminated by a far off-resonance laser beam (pump beam) with frequency ω and wavevector $\vec{k}$ directed along its axial direction. After backscattering of photons with $\vec{k}_s \simeq -\vec{k}$ and the subsequent recoil of atoms, a matter wave grating forms, due to the quantum interference between the two momentum components of the wavefunction of the condensate. The effect of this grating is to further scatter the incident light in a self-amplifying process.

collisions, may seriously inhibit the CARL process and destroy the coherence in the matter wave field [8]. The control of decoherence in the photon-BEC interaction would be a significant step toward the achievement of macroscopic entanglement of coherent matter waves. In this paper we investigate both theoretically and experimentally the influence of the initial velocity of the condensate on superradiant Rayleigh scattering [9].

Our system consists of an elongated BEC of rubidium atoms exposed to a single off-resonant laser pulse (pump beam) directed along the condensate symmetry axis (see figure 1). The laser is far detuned from any atomic resonance and the only scattering mechanism present is Rayleigh scattering [2]. In an elongated condensate a preferential direction for the scattered photons emerges, causing superradiant Rayleigh scattering. In this regime the atoms, initially scattered randomly, interfere with the atoms in the original momentum state creating a matter-wave grating with the right periodicity to further scatter the laser photons in the same mode. Both the matter-wave grating and the scattered light are then coherently amplified. In our geometry photons are back-scattered with $\vec{k}_s \approx -\vec{k}$, where $\vec{k}$ is the wave-vector of the laser photon, and the atoms move away from the original condensate with a relative momentum $2\hbar k$ in the direction of the laser beam. The efficiency of the process is limited by the decoherence between the original and the recoiled atomic wavepackets, causing damping of the matter-wave grating. We identify two different mechanisms for decoherence. One results from Doppler and mean field broadening of the matter wave field [2, 10] and the other is due to phase diffusion. The latter mechanism, dependent on the energy separation between the initial and final states of the system [11, 12], can be controlled by initially setting the condensate into motion. In particular, we observe that phase diffusion decoherence vanishes when the initial condensate momentum is such that the scattered atomic wavepacket has the same kinetic energy of the unscattered condensate in the laboratory frame.

On the other hand, when counterpropagating laser beams are used, light forms a periodic structure on which the matter wave can perform Bragg scattering. Indeed, this process too is coherent and the condensate undergoes Rabi oscillations between different momentum states. We study the transition between the aforementioned superradiant regime and the Rabi oscillations regime by introducing a small amount of laser light (seed beam) counterpropagating with respect to the pump beam.

The paper is organized as follows. In section 2 we introduce the CARL-BEC model. In section 3 we describe the experimental setup and compare the

experimental results on superradiance from a moving BEC with the theoretical model. In section 4 we explore the transition from the superradiant regime to the Rabi oscillations regime induced by adding a weak counterpropagating laser beam.

2. Theoretical analysis

The evolution of the system in this regime is described by the 1-D CARL-BEC model, i.e. a Gross-Pitaevskii model generalized to include the self-consistent evolution of the scattered radiation amplitude:

$$i\frac{\partial\Psi}{\partial t} = -\frac{\hbar}{2m}\frac{\partial^2\Psi}{\partial z^2} + \beta N|\Psi|^2\Psi + ig\left\{a^* e^{i(2kz-\delta t)} - \text{c.c.}\right\}\Psi, \tag{1}$$

$$\frac{\mathrm{d}a}{\mathrm{d}t} = gN\int \mathrm{d}z|\Psi|^2 e^{i(2kz-\delta t)} - \kappa a. \tag{2}$$

In equations (1) and (2), $a = (\epsilon_0 V/2\hbar\omega_s)^{1/2}E_s$ is the dimensionless electric field amplitude of the scattered beam with frequency ω_s, $g = (\Omega/2\Delta)\times(\omega d^2/2\hbar\epsilon_0 V)^{1/2}$ is the coupling constant, Ω is the Rabi frequency of the laser beam with a frequency ω detuned from the atomic resonance frequency ω_0 by $\Delta = \omega - \omega_0$, $d = \hat{\epsilon}\cdot\vec{d}$ is the electric dipole moment of the atom along the polarization direction $\vec{\epsilon}$ of the laser, V is the volume of the condensate, N is the total number of atoms in the condensate and $\delta = \omega - \omega_s$. The matter wave field is normalized such that $\int \mathrm{d}z|\Psi|^2 = 1$. The second term in the right hand side of equation (1) describes the atom-atom interaction due to binary collisions, where $\beta = 4\pi\hbar a_s/m\Sigma$, a_s is the scattering length and Σ is the condensate cross section. This term can be neglected since the experiment has been performed after expansion. The last term in the right-hand side of equation (1) represents the self-consistent optical wave grating, whose amplitude depends on time according to equation (2), while the first term in the right-hand side of equation (2) represents the self–consistent matter-wave grating. Equation (2) has been written in the ''mean-field'' limit, which models the propagation effects with a damping term where $\kappa \approx c/2L$ and L is the condensate length [13].

If the condensate is much longer than the radiation wavelength and approximately homogeneous, then periodic boundary conditions can be assumed and the wavefunction can be written as

$$\Psi(z,t) = \sum_n c_n(t)u_n(z)e^{-in\delta t}, \tag{3}$$

where $u_n(z) = (2/\lambda)^{1/2}\exp(2ink z)$ are the momentum eigenstates

$$\hat{p}_z u_n(z) = p_z u_n(z), \tag{4}$$

with eigenvalues $p_z = n(2\hbar k)$. Introducing the density operator

$$\hat{\rho} = \sum_{m,n}\rho_{m,n}|m\rangle\langle n|, \tag{5}$$

where $\rho_{m,n} = c_m c_n^*$, $\omega_n = 4\omega_R n^2 - \delta n$ and $\hat{p} = \hat{p}_z/(2\hbar k)$ is the normalized momentum operator with, in a Fock representation, eigenstates $|n\rangle$ and eigenvalues n. From equations (1) and (2) we obtain:

$$\frac{\mathrm{d}\rho_{m,n}}{\mathrm{d}t} = -i(\omega_m - \omega_n)\rho_{m,n} + g[a(\rho_{m,n-1} - \rho_{m+1,n}) + a^*(\rho_{m-1,n} - \rho_{m,n+1})] - \frac{\tau}{2}(\omega_m - \omega_n)^2 \rho_{m,n}, \tag{6}$$

$$\frac{\mathrm{d}a}{\mathrm{d}t} = gN \sum_n \rho_{n,n+1} - \kappa a. \tag{7}$$

The last term added in equation (6) describes a phase-diffusion decoherence process, whose amplitude is characterized by a constant τ. This term, fundamental in describing our experimental results, arises from a δ-correlated gaussian noise on the eigen-energies of the system and causes the decay of the off-diagonal matrix elements, so that the density matrix becomes diagonal in the basis of the recoil momentum states. This decoherence in the superposition state causes the decay of the matter wave grating resulting from the quantum interference of the two momentum components. Therefore the self amplifying process for the backscattered radiation is stopped. Equation (6) may be written as a master equation [15] for the density operator $\hat{\rho}$:

$$\frac{\mathrm{d}\hat{\rho}}{\mathrm{d}t} = -\frac{i}{\hbar}[\hat{H}, \hat{\rho}] - \frac{\tau}{2}\hbar^2[\hat{H}_0, [\hat{H}_0, \hat{\rho}]], \tag{8}$$

where $\hat{H} = \hat{H}_0 + \hat{V}$, $\hat{H}_0 = 4\hbar\omega_R \hat{p}^2 - \hbar\delta\hat{p}$ and $\hat{V} = i\hbar g(a^* e^{2ikz} - h.c.)$. The phase destroying term with the double commutator of the Lindblad form in the right-hand side of equation (8) generates the damping term added in equation (6). This term appeared in many models of decoherence and induces diffusion in variables that do not commute with the Hamiltonian, preserving the number of atoms in the condensate. In this term we have neglected the interaction $\hat{V}$ in the weak-coupling limit $g^2 N/\kappa \ll \omega_R$.

In our experimental conditions the superradiant Rayleigh scattering involves only neighboring momentum states, i.e. transitions from the initial momentum state $p_0 = n(2\hbar k)$ to the final momentum state $(n+1)2\hbar k$. In this limit, the system is equivalent to a two-level system and equations (6) and (7) reduce to the Maxwell-Bloch system [10, 16]:

$$\frac{\mathrm{d}S}{\mathrm{d}t} = gAW - \gamma_n S, \tag{9}$$

$$\frac{\mathrm{d}W}{\mathrm{d}t} = -2g(AS^* + h.c.), \tag{10}$$

$$\frac{\mathrm{d}A}{\mathrm{d}t} = gNS - (\kappa - i\Delta_n)A, \tag{11}$$

where $S = \rho_{n,n+1} e^{-i\Delta_n t}$, $A = a e^{-i\Delta_n t}$, $W = P_n - P_{n+1}$ is the population fraction difference between the two states (where $P_n = \rho_{n,n}$ and $P_n + P_{n+1} = 1$),

$$\Delta_n = \omega - \omega_s - 4\omega_R(2n+1), \tag{12}$$

is the detuning from the Bragg resonance with the scattered field (i.e. the condition for energy conservation) and the decoherence rate γ_n is given by:

$$\gamma_n = \gamma_0 + \frac{\tau}{2}\Delta_n^2 = \gamma_0 + \frac{\tau}{2}\left[\omega - \omega_s - 4\omega_R\left(\frac{p_0}{\hbar k} + 1\right)\right]^2. \tag{13}$$

To the decoherence rate γ_n we have added an extra term γ_0 taking into account other coherence decay mechanisms, for example Doppler and inhomogeneous broadenings of the two-photon Bragg resonance [2, 10]. We note that in equation (11), S represents half of the amplitude of the matter-wave grating. In fact, if

$$\Psi \approx c_n u_n(z) + c_{n+1} u_{n+1}(z), \tag{14}$$

the longitudinal density is

$$|\Psi|^2 \approx (2/\lambda)\{1 + 2\mathrm{Re}[S^* \exp(2ikz)]\}, \tag{15}$$

which describes a matter wave grating with a periodicity of half the laser wavelength. The main result is that the second term of equation (13), arising from a phase diffusion decoherence mechanism, depends on the frequency detuning between the incident and scattered radiation beams and on the initial momentum of the condensate, $p_0 = n(2\hbar k)$. We observe that the velocity-dependent term of the decoherence rate is invariant under Galilean transformation. In fact, in a frame moving with respect to the laboratory frame, the shift of p_0 compensates the Doppler shift of the frequency difference $\omega - \omega_s$.

The parameters used in the experiment match those for the superfluorescent regime [14], in which the field loss rate κ is much larger than the coupling rate $g\sqrt{N}$. In this regime, for $t \gg \kappa^{-1}$ we can perform an adiabatic elimination putting $\mathrm{d}A/\mathrm{d}t = 0$ so that

$$A \simeq \frac{gNS}{(\kappa - i\Delta_n)}. \tag{16}$$

The analytical solution for the fraction of atoms with initial momentum $p_0 = n(2\hbar k)$ is

$$P_n = 1 - \frac{1}{2}\left(1 - \frac{2\gamma_n}{G}\right)\left\{1 + \frac{1}{2}\tanh[(G - 2\gamma_n)(t - t_0)]\right\}, \tag{17}$$

where

$$G = \frac{2g^2 N\kappa}{\left(\kappa^2 + \Delta_n^2\right)}, \tag{18}$$

is the superradiant gain and t_0 is a delay time. Furthermore, in our experiment $\kappa \gg \Delta_n$. Therefore $G \approx 2g^2N/\kappa$, and independent from the atomic velocity. Equation (17) assumes the threshold condition $G > 2\gamma_n$ i.e. the gain must be larger than the decoherence rate.

3. Experimental setup and results

The experiment is performed with a cigar-shaped condensate of ^{87}Rb produced in a Ioffe-Pritchard magnetic trap by means of RF-induced evaporative cooling. The axial and radial frequencies of the trap are $\omega_z/2\pi = 8.70(7)\,\mathrm{Hz}$ and $\omega_r/2\pi = 90.1(4)\,\mathrm{Hz}$ respectively, with the z-axis oriented horizontally. After the

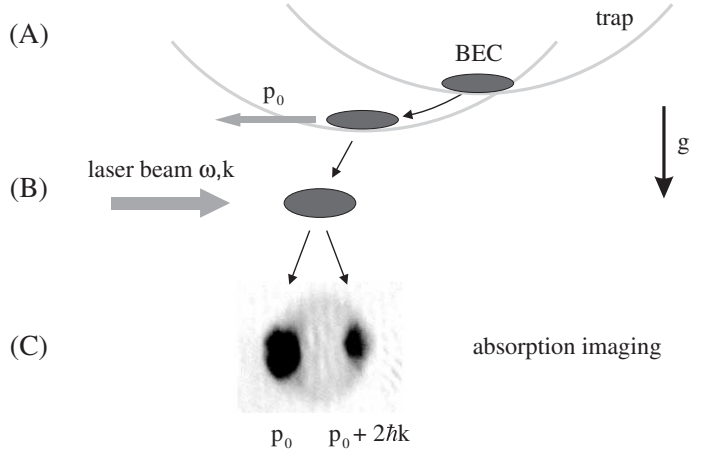

Figure 2. Schematic of the experimental procedure. The condensate is set into motion by a sudden displacement of the magnetic trap center (A). When the condensate reaches the desired momentum p_0 we switch off the magnetic trap and flash the atoms with a far off resonance laser pulse directed along the condensate symmetry axis (B). After an expansion time allowing a complete separation of the momentum components p_0 and $p_0 + 2\hbar k$ (28 ms) we take an absorption image of the atoms (C).

evaporative ramp, a collective dipole motion of the condensate inside the harmonic potential is induced along the z-axis, allowing tuning of the atomic velocity. The dipole oscillation is excited by non-adiabatically displacing the center of the magnetic trap. When the condensate has reached the maximum velocity in the magnetic potential, the trap is suddenly switched off and the cloud expands with a horizontal velocity proportional to the displacement of the trap (see figure 2). A square pulse of light along the z-axis is applied 2 ms after the release of the condensate. At this time the magnetic field of the trap is completely switched off and the atomic cloud still has an elongated shape. After 2 ms of free expansion the radial and axial sizes of the condensate are typically 10 and 70 μm, respectively. The pulse length is controlled with an acousto-optic modulator. The light comes from a diode laser red-detuned 13 GHz away from the rubidium D2 line at $\lambda = 780\,\text{nm}$ and has an intensity of $1.35\,\text{W/cm}^2$ corresponding to a Rayleigh scattering rate of roughly $5\times10^2\,\text{s}^{-1}$. The linearly polarized laser beam is collimated and aligned along the z-axis of the condensate. In this geometry the superradiant light is backscattered and the self-amplified matter-wave propagates in the same direction as the incident light. After an expansion of 28 ms, when the two momentum components are spatially separated, an absorption image of the cloud along the horizontal radial direction is taken. In order to minimize spurious reflections the laser beam has been aligned at a nonzero angle with respect to the normal to the vacuum cell windows. In section 5 we will discuss in detail the possible effect of some counterpropagating light seeding the superradiant process.

In figure 2C we show a typical absorption image in which the left peak is the condensate in its original momentum state p_0 and the right peak is formed by atoms recoiling after the superradiant scattering at $p_0 + 2\hbar k$. The spherical halo centered between the two density peaks is due to non-enhanced spontaneous processes, i.e. random isotropic emission following the absorption of one laser photon. From a 2D-fit of the pictures assuming a Thomas-Fermi density

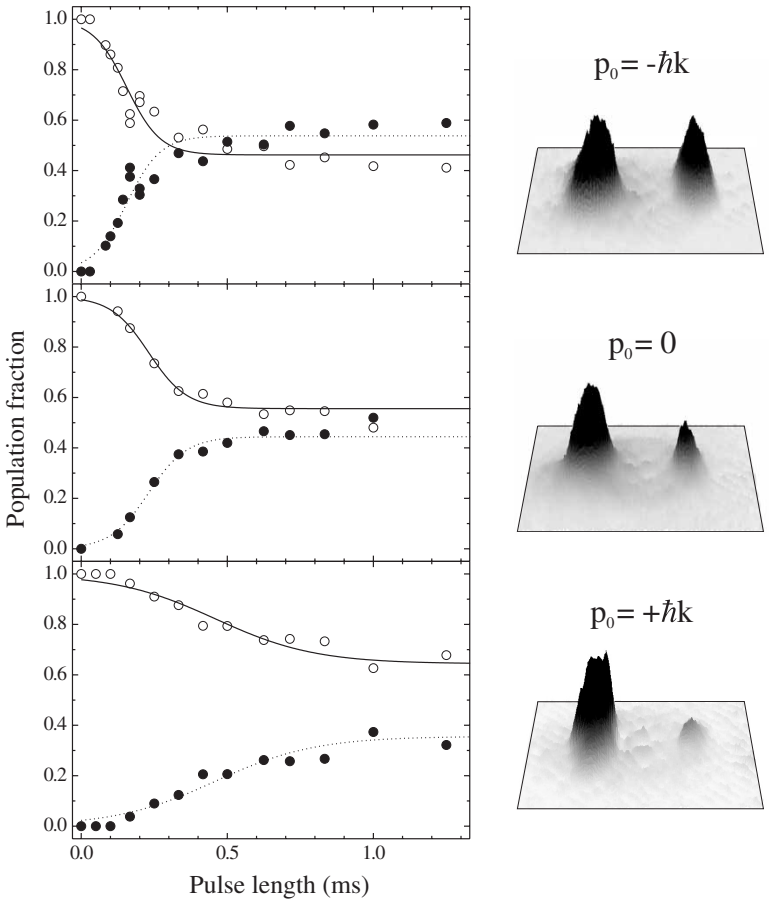

Figure 3. Left, time evolution of population in the original condensate (open circles) and in the recoiled wavepacket (filled circles) for different pulse durations. The solid line is a fit to the hyperbolic tangent (17) predicted by the theoretical model, the dotted line is simply one minus the fit curve. The momentum of the original condensate is set to $-\hbar k$ (top), 0 (center) and $+\hbar k$ (bottom). Right, plots of the atomic density profile after interaction with a 250 μs pulse for the three cases of original momentum as on the left. The laser detuning and intensity are 13 GHz and 1.35 W/cm^2 respectively.

distribution we extract the number of atoms in both the original and the recoiled peaks. We study the population in the two momentum peaks as a function of the duration of the laser pulse for different initial velocities of the condensate.

In figure 3 we report the experimental results for the population fractions of the initial wavepacket, P_n, and of the scattered wavepacket, P_{n+1}, as functions of the laser pulse duration for three different initial momenta p_0. The continuous lines represent the fit with the theoretical function of equation (17). From the fits we extract the values of G and γ_n for different p_0. The measured value of $G = 19(3)\,\mathrm{ms}^{-1}$ does not appreciably depend on p_0, as expected from the theoretical treatment. In contrast, for the decoherence rate γ_n we observe a strong dependence on the initial momentum p_0.

In figure 4 we plot the experimental points for the decoherence rate γ_n as a function of the initial momentum of the atoms. The data show a parabolic behavior

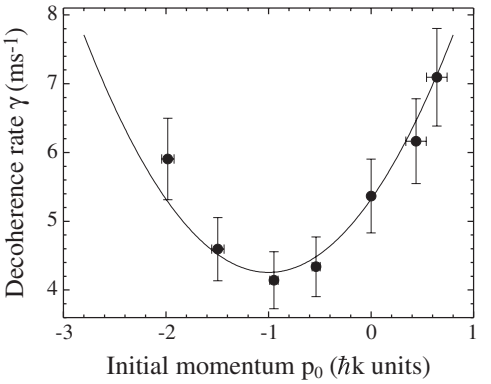

Figure 4. Decoherence rate as a function of the initial momentum of the condensate. The solid line is a fit of the experimental data with a parabola centered in $p_0 = -\hbar k$, as expected from the theoretical model.

in good agreement with the prediction of equation (13) assuming $\omega = \omega_s$ in the laboratory frame. Fitting the data with the theoretical curve we obtain the values $\gamma_0 = 4.2(2)\ \mathrm{ms}^{-1}$ and $\tau = 2.4(2) \times 10^{-7}\ \mathrm{s}$. We remark that the expected linewidth of the Bragg resonance [17] for our experimental parameters is $\gamma_0 \approx 3\ \mathrm{ms}^{-1}$, close to the value obtained from the fit. Notice that the decoherence rate is minimized for $p_0 = -\hbar k$. Indeed, if the initial momentum is $-\hbar k$, after scattering the atoms have the same kinetic energy in the laboratory frame and, with the above assumption for the scattered light frequency ω_s, the phase destroying decoherence term in (8) is zero. This identifies a subspace which is decoherence free with respect to the phase destroying process [18].

4. Seeding the superradiance

In this paragraph we discuss experiments performed adding a counterpropagating laser beam (seed beam) ''stimulating'' the superradiant scattering. This allowed us to investigate the crossover from the superradiant amplification of light to the Rabi oscillations regime due to the Bragg scattering induced by the presence of the two laser beams. The scheme of the experiment is the same as the one presented above, with the only difference that now the condensate is illuminated by two beams coming from opposite directions. In these measurements the condensate was at rest in the laboratory frame ($p_0 = 0$) and the seed frequency ω_s was detuned from the pump frequency ω by $\Delta\omega \equiv \omega - \omega_s = 4\omega_R$ in order to satisfy the Bragg resonance condition $\Delta_0 = 0$. In order to provide the right detuning, the two laser beams were modulated by two independent acousto-optic modulators (AOM) driven by two different phase-locked carrier frequencies.

In these conditions equations (9–11) become

$$\frac{\mathrm{d}S}{\mathrm{d}t} = gAW - \gamma_n S, \tag{19}$$

$$\frac{\mathrm{d}W}{\mathrm{d}t} = -2g(AS^* + h.c.), \tag{20}$$

$$\frac{\mathrm{d}A}{\mathrm{d}t} = gNS + i\Delta_n A - \kappa(A - A_{in}), \tag{21}$$

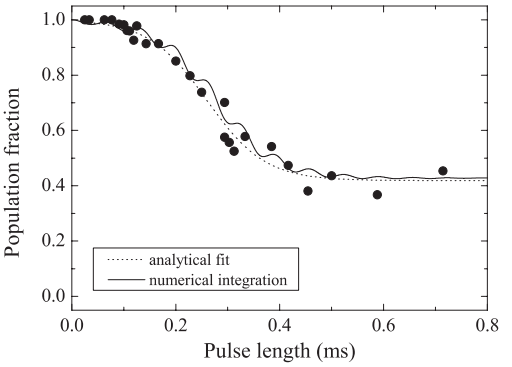

Figure 5. Time evolution of the population of the condensate with $p_0 = 0$ as a function of the superradiant pulse length. The experimental data are fitted to the analytical curve of equation (17) (dotted line). The continuous line is the result of the numerical integration of equations (19)–(21).

where A_{in} is the scaled amplitude of the seed. In the presence of a seed the dynamics of the system shows a competition between two kinds of phenomena: the CARL evolution when A_{in} is small enough, and Rabi oscillations when A_{in} becomes dominant. We can obtain an analytical solution of this system in the two limiting cases of $A_{in} = 0$ and $A_{in} \gg A$. The first case has been previously illustrated and its analytic solution is reported in equation (17). In the second case the solution for the population fraction becomes, for $\Delta_n = 0$ and $\gamma_n = \gamma_0$,

$$P_n = \frac{1}{2}\left\{1 + e^{-\gamma_0(t-t_0)/2}\left[\cos\Omega(t-t_0) + \frac{\gamma_0}{2\Omega}\sin\Omega(t-t_0)\right]\right\}, \tag{22}$$

where $\Omega = \sqrt{\Omega_0 - \gamma_0^2/4}$ and $\Omega_0 = 2gA_{in}$ is the Rabi frequency of the input signal. In equation (22) we have added a phenomenological delay time t_0 to account for shifts in the experimental timing. In the intermediate regime we have to resort to a numerical integration of equations (19)–(21).

In order to test the results of the numerical integration, we first present in figure 5 data referring to an experiment performed without seed, when the superradiance starts from noise. The effect of the noise is introduced in the model as an injected signal with frequency $\omega_s = \omega$. The comparison with the experimental results allows us to determine the amplitude of the noise which triggers the onset of the superradiant process. The data in figure refers to an experiment performed with a pump beam intensity $I_0 = 0.9$ W/cm^2 and detuning 15 GHz. The dotted line is a fit of the experimental data to the curve of equation (17) giving $G = 31$ ms^{-1}, $\gamma_n = 6.44$ ms^{-1} and $t_0 = 0.26$ ms as best parameters. The continuous line is instead the result of the numerical integration of equations (19)–(21) where we assume an injected signal with a Rabi frequency $\Omega_0 = 9.7$ ms^{-1} corresponding to an equivalent intensity of $I_N = 1.1$ μW/cm^2. This value is chosen in such a way that the simulation has the best agreement with the experimental data. We define this value of the intensity as the ''equivalent input noise'' for this experimental setup. We explain the oscillating behavior of the continuous line as an effect of the finite value of Δ_0 when $\omega = \omega_s$.

We discuss now the results of the experiment performed varying the seed beam intensity I_s. In figure 6 we show data obtained ranging the seeding intensity from

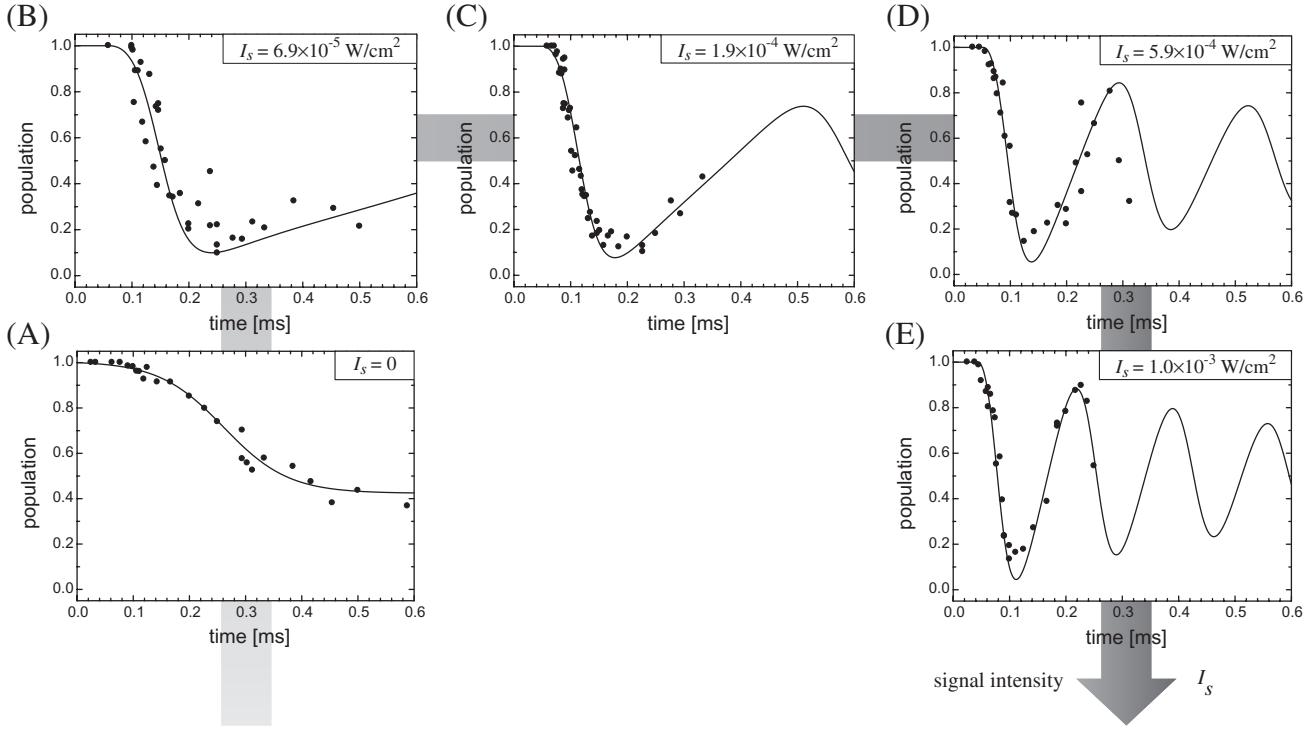

Figure 6. Time evolution of the population of the condensate at $p_0 = 0$ interacting with the superradiant pump beam and a counterpropagating seed beam (resonant with the Bragg transition $\Delta\omega = 4\omega_R$) for different intensities. As the intensity increases (clockwise) the system goes from a superradiant regime to a Rabi oscillations regime.

$I_s = 7 \times 10^{-5}$ W/cm^2 to $I_s = 1 \times 10^{-3}$ W/cm^2. We observe that in this configuration the dynamics of the system goes from pure superradiant amplification of light (showing the typical tanh-like behaviour) to almost pure damped Rabi oscillations of population. Note that in the intermediate regime we observe some damped asymmetric oscillations of population, in which the building up of the scattered peak is faster than its decreasing, as a result of the interplay between the two processes. In figure 6E the experimental data are fitted with the analytic curve of equation (22) describing the Rabi oscillations regime, while in figure 6B, C, D the experimental results in the intermediate regime are compared with the numerical solution of equations (19)–(21). The parameters used in the numerical solution are the ones obtained from the fits of the data in figure 5 and figure 6E corresponding to the two limiting cases (pure superradiance and pure Rabi oscillations) for which analytical solutions exist.

We now go back to discuss the role played by backdiffused light in the experiment described in the previous section. In an experimental apparatus it is very difficult to avoid the presence of light backreflected by the vacuum cell windows. In particular, considering the 1D geometry of our experiment, if some counterpropagating light exists, in the case $p_0 = -\hbar k$ this could cause stimulated Raman Bragg scattering of atoms in the same direction and with the same transfer of momentum $2\hbar k$, thus masking the effect of a pure superradiant scattering. Indeed, in our experimental setup we detected the backdiffusion of a small amount of light, caused by the poor quality of the cell windows. We first estimated the magnitude of this light directly measuring with a power-meter the intensity backscattered collinearly to the pump light. This intensity is 7×10^{-6} W/cm^2, corresponding to $\simeq 8 \times 10^{-6}$ of the pump intensity. The effect of this small amount of backdiffused light has also been evidenced performing the measurements without seed in the far-detuned regime. In this situation the spontaneous process triggering the superradiant amplification is suppressed (its rate being proportional to $1/\Delta^2$), while the stimulated Raman Bragg scattering can be predominant (its rate being proportional to $1/\Delta$, as can be seen in figure 7), provided that some counterpropagating light exists. Indeed, in this regime (for $\Delta \simeq 150$ GHz, $I \simeq 3$ W/cm^2 and $\Delta t \simeq 0.5$ ms), for an initial momentum $p_0 = +\hbar k$, we observe the signature of a small Bragg scattering at $p = -\hbar k$ (i.e. in the direction opposite to the superradiant scattering), that can be explained only assuming a backreflected light of 1.2×10^{-5} W/cm^2. These two independent observations confirm that, in all the experiments described above, we should take into account the presence of some counterpropagating light at the same frequency ω of the pump and a relative intensity of $\simeq 10^{-5}$.

Coming back to the experiment on pure superradiant scattering, the spurious light backdiffused by the cell windows (approximately a fraction 10^{-5} of the pump light) is small enough to allow safely to state that all the measurements discussed in section 3 have been made in a regime in which the dynamics of the system is completely dominated by superradiance. This amount of light is actually of the same order of magnitude as the equivalent input noise triggering the superradiant process. This can justify the assumption $\omega_s = \omega$ used to fit the experimental data of figure 4. We remark that the presence of the backdiffused light cannot explain our results in terms of Bragg scattering, since the width of the Bragg resonance is one order of magnitude smaller than the range of momenta explored in our experiment and shown in figure 4 (so that only the

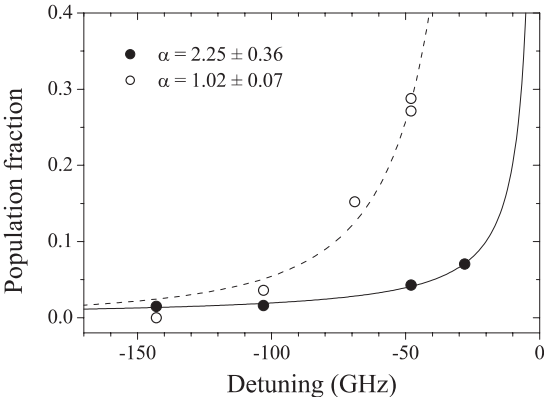

Figure 7. Comparison between superradiant scattering and Bragg scattering. In the graph we show the population of the scattered peak as a function of the pump beam detuning from the atomic resonance. The filled circles refer to superradiant scattering, while the open circles refer to stimulated Bragg scattering. The curves are fits to the experimental data with a $1/\Delta^{\alpha}$ function. The exponents obtained from the fits are consistent with the ones expected from the theory: $\alpha = 2$ for superradiance and $\alpha = 1$ for Bragg transitions. The two curves should not be directly compared, because obtained with different laser parameters (intensity and pulse duration). Note that the efficiency of the superradiant process approaches zero faster than the Bragg scattering efficiency.

experimental point at $p_0 = -\hbar k$ would be affected). Furthermore, the hyperbolic tangent dependence of the atomic population in figure 3 can only be explained by the self consistent amplification of the matter wave grating and of the backscattered light as described in the CARL-BEC model.

5. Conclusions

In conclusion, we have studied superradiant light scattering from a moving Bose-Einstein condensate. We have introduced the CARL-BEC model, showing that the efficiency of the overall process is fundamentally limited by the decoherence between the two atomic momentum states. In a first experiment we have studied the dependence of the decoherence rate on the initial momentum of the condensate. We identify a velocity dependent contribution to the decoherence rate, which can be minimized when the energy conservation condition is satisfied (i.e. the scattered and the unscattered atomic wavepacket have the same kinetic energy in the laboratory frame). In a second experiment, performed adding a counter-propagating beam, we have explored the transition from the pure superradiant regime to the Rabi oscillations regime induced by stimulated Bragg scattering. The theoretical model is in good agreement with the experimental results for the intermediate regime.

The fully quantized version of the CARL-BEC model offers the possibility of investigating the realisation of macroscopic atom-atom or atom-photon entanglement [5, 6]. In particular, the control of decoherence obtained in this work represents a significant step in this direction.

Acknowledgements

This work has been supported by the EU, INFM and MIUR. We thank L. De Sarlo and R. Saers for their active participation in the experimental part of the work and B. Englert and S. Olivares for useful discussions. We also thank J. E. Lye for a careful reading of the manuscript.

References

[1] See for example Inguscio, M., Wieman, C. E., and Stringari, S., 1999, *Bose-Einstein Condensation in Atomic Gases* (Amsterdam, Oxford, Tokyo, Washington: IOS Press).
[2] Inouye, S., Chikkatur, A. P., Stamper-Kurn, D. M., Stenger, J., Pritchard, D. E., and Ketterle, W., 1999, *Science*, **285,** 571.
[3] Kozuma, M., Suzuki, Y., Torii, Y., Sugiura, T., Kuga, T., Hagley, E. W., and Deng, L., 1999, *Science*, **286,** 2309; Inouye, S., Pfau, T., Gupta, S., Chikkatur, A. P., Gorlitz, A., Pritchard, D. E., and Ketterle, W., 1999, *Nature*, **402,** 641.
[4] Bonifacio, R., and De Salvo, L., 1994, *Nucl. Instrum. Methods Phys. Res.* A, **341,** 360; Bonifacio, R., De Salvo, L., Narducci, L. M., and D'Angelo, E. J., 1994, *Phys. Rev.* A, **50,** 1716.
[5] Moore, M. G., Zobay, O., and Meystre, P., 1999, *Phys. Rev.* A, **60,** 1491.
[6] Piovella, N., Cola, M., and Bonifacio, R., 2003, *Phys. Rev.* A, **67,** 013817.
[7] Vogels, J. M., Xu, K., and Ketterle, W., 2002, *Phys. Rev. Lett.*, **89,** 020401.
[8] Gasenzer, T., Roberts, D. C., and Burnett, K., 2002, *Phys. Rev.* A, **65,** 021605R.
[9] Bonifacio, R., Cataliotti, F. S., Cola, M., Fallani, L., Fort, C., Piovella, N., and Inguscio, M., preprint, http://arxiv.org/abs/cond-mat/0306500.
[10] Inouye, S., Low, R. F., Gupta, S., Pfau, T., Gorlitz, A., Gustavson, T. L., Pritchard, D. E., and Ketterle, W., 2000, *Phys. Rev. Lett.*, **85,** 4225.
[11] Zurek, W. H., 1981, *Phys. Rev.* D, **24,** 1516.
[12] Bonifacio, R., 1999, *Il Nuovo Cimento* B, **114,** 473.
[13] Bonifacio, R., Schwendimann, P., and Haake, F., 1971, *Phys. Rev.*, **A 4,** 302; 1971, **4,** 854.
[14] Bonifacio, R., and Lugiato, L. A., 1975, *Phys. Rev.*, **A 11,** 1507.
[15] Walls, D. F., and Milburn, G. J., 1985, *Phys. Rev.*, **A 31,** 2403.
[16] Piovella, N., Gatelli, M., and Bonifacio, R., 2001, *Optics Comm.*, **194,** 167.
[17] Stenger, J., Inouye, S., Chikkatur, A. P., Stamper-Kurn, D. M., Pritchard, D. E., and Ketterle, W., 1999, *Phys. Rev. Lett.*, **82,** 4569.
[18] See for example De Martini, F., and Monroe, C., 2003, *Experimental Quantum Computation and Information* (Amsterdam, Oxford, Tokyo, Washington: IOS Press).
[19] Cola, M., 2003, PhD Thesis, University of Milan.